Engineering Optimization

ISSN: 0305-215X (Print) 1029-0273 (Online) Journal homepage: http://www.tandfonline.com/loi/geno20

Design optimization of an artificial lateral line system incorporating flow and sensor uncertainties

Ali Ahrari, Hong Lei, Montassar Aidi Sharif, Kalyanmoy Deb & Xiaobo Tan

To cite this article: Ali Ahrari, Hong Lei, Montassar Aidi Sharif, Kalyanmoy Deb & Xiaobo Tan (2017) Design optimization of an artificial lateral line system incorporating flow and sensor uncertainties, Engineering Optimization, 49:2, 328-344, DOI: 10.1080/0305215X.2016.1168108

To link to this article: http://dx.doi.org/10.1080/0305215X.2016.1168108

Published online: 13 Apr 2016.

ENGINEERING OPTIMIZATION, 2017
VOL. 49, NO. 2, 328–344
http://dx.doi.org/10.1080/0305215X.2016.1168108

Taylor & Francis
Taylor & Francis Group

Design optimization of an artificial lateral line system incorporating flow and sensor uncertainties

Ali Ahrari[a], Hong Lei[b], Montassar Aidi Sharif[b], Kalyanmoy Deb[b] and Xiaobo Tan[b]

[a]Department of Mechanical Engineering, College of Engineering, Michigan State University, East Lansing, MI, USA; [b]Department of Electrical and Computer Engineering, College of Engineering, Michigan State University, East Lansing, MI, USA

ABSTRACT

An artificial lateral line (ALL) system consists of a set of flow sensors around a fish-like body. An ALL system aims to identify surrounding moving objects, a common example of which is a vibrating sphere, called a dipole. Accurate identification of a vibrating dipole is a challenging task because of the presence of different types of uncertainty in measurements or in the underlying flow model. Proper selection of design parameters of the ALL system, including the shape, size, number and location of the sensors, can highly influence the identification accuracy. This study aims to find such an optimum design by developing a specialized bi-level optimization methodology. It identifies and simulates different sources of uncertainty in the problem formulation. A parametric fitness function addresses computational and practical goals and encompasses the effect of different sources of uncertainty. It can also analyse the trade-off between localization accuracy and the number of sensors. Comparison of the results for different extents of uncertainty reveals that the optimized design strongly depends on the amount of uncertainty as well as the number of sensors. Consequently, these factors must be considered in the design of an ALL system. Another highlight of the proposed bi-level optimization methodology is that it is generic and can be readily extended to solve other noisy and nested optimization problems.

ARTICLE HISTORY
Received 18 January 2016
Accepted 15 March 2016

KEYWORDS
uncertainty formulation; dipole source localization; bi-level optimization; sensor placement

1. Introduction

The lateral line system is an important flow-sensing organ, which is involved in various behaviours of fish (Bleckmann 1994), such as schooling (Pitcher, Partridge, and Wardle 1976), station holding (Bleckmann *et al.* 2012) and object detection (Von Campenhausen, Riess, and Weissert 1981). A lateral line system consists of arrays of flow sensors called neuromasts (Hassan 1993). One of the two types of neuromasts is the superficial neuromasts, which stick out of the fish skin and respond to flow velocities (Engelmann *et al.* 2000). The response of the neuromasts, in the form of neuronal pulses, is further transmitted to the central nervous system for information processing (Bleckmann 2008).

It is of great interest to develop an engineering equivalent of a biological lateral line for underwater applications. Such an artificial lateral line (ALL) system will introduce a novel and noiseless sensing modality for the navigation and control of underwater robots and vehicles (DeVries *et al.* 2015), and

CONTACT Ali Ahrari aliahrari1983@gmail.com

provide complementary information to traditional underwater vision sensors and sonar (Fernandez *et al.* 2011).

Some theoretical work has been conducted on flow modelling and information processing to extract information in ALLs (Hassan 1993; Ren and Mohseni 2012; DeVries and Paley 2013). Although some previous studies aimed at detecting moving objects and vortices (Venturelli *et al.* 2012; Chambers *et al.* 2014), most of them focused on localization of a vibrating source, called the dipole source. The dipole source emulates the rhythmic movement of fish body and fins, and has been commonly used as a biological stimulus such as counter-specific, predator or prey (Coombs and Conley 1997a, 1997b). Dipole source localization has also played an important role in the development of ALLs, detection and estimation of nearby fish-like robots, and coordination and control of underwater robots (Dagamseh *et al.* 2010; Abdulsadda and Tan 2012).

Although many studies have been conducted on localization of a dipole source using the ALL system (Dagamseh *et al.* 2010; Yang *et al.* 2010; Abdulsadda and Tan 2011, 2012, 2013), very few have addressed the identification of an optimal ALL, the one that provides maximum localization accuracy for an arbitrary dipole. Once the ALL is identified, the next task is to locate a finitely specified number of sensors on the ALL. In a previous study (DeVries and Paley 2013), observability-based optimization of placement of flow sensors was discussed for control purposes. The estimation and optimization were conducted in a uniform flow field, which was different from the localization of a dipole source. Furthermore, the flow model employed was commonly assumed to be accurate, although, like most other theoretically driven models, it depends on assumptions that may not be satisfied in practical situations.

Ahrari *et al.* (2015) proposed a parametric fitness function for measuring the accuracy of an ALL in the presence of uncertainties. The purpose of the ALL was to identify the maximum velocity and direction of vibration in addition to the coordinates of the dipole. A bi-level optimization method was developed to find the optimal ALL such that the accuracy of identification for an arbitrary dipole source is maximized. Unlike previous studies, which either ignored uncertainties or considered only sensor uncertainty, both flow model and sensor uncertainty were formulated and simulated in the optimization process. Furthermore, the design optimization of the ALL was not limited to location of the sensors, but also included the shape and size of the ALL. Starting with a previous preliminary study (Ahrari *et al.* 2015), this article focuses on the following aspects.

- The trade-off between computation time and quality of the lower loop is investigated by exploring the effect of intervening parameters. Based on the study, an appropriate parameter setting is proposed for subsequent studies.
- A few additional practicalities on the design of the ALL system are imposed, including a lower bound on the shape of ALL, to prevent designs that are not practical.
- The dependence of the optimal ALL system on the extent of uncertainty in the model and sensor measurements is investigated.
- The results of a widely adopted multi-objective optimization method are compared with the state-of-the-art generative single-objective optimization to clearly understand the trade-off between the number of sensors and obtained localization accuracy.

The rest of this article is organized as follows. In Section 2, the dipole identification problem is formulated. Different sources of uncertainties, including the flow model uncertainty and the sensor measurement uncertainty are discussed and estimated. In Section 3, the proposed bi-level optimization method is detailed, including the development of a robust parametric fitness function for measuring the accuracy of the ALL system in the presence of uncertainties. Numerical results are then provided and discussed in Section 4. Finally, conclusions are drawn in Section 5 and prospective future studies of this research are highlighted.

2. Problem outline

In this study, discussion is limited to a two-dimensional setting. In particular, an ALL system is considered to consist of a cylindrical body with fish-shaped cross-section and multiple sensors that measure the local flow velocity around the body (see a prototype illustration in Figure 1a). In theory, it is assumed that the cylindrical body has infinite height and the flow is restricted to the plane of its cross-section. Consequently, the body configuration is fully captured by the size and shape of the cross-section.

2.1. Flow model

With a given flow model, the flow velocity at any location (x_k, y_k) can be computed if the parameters of the dipole source, including its maximum velocity of vibration (A), orientation angle of vibration (β) and location of the dipole (x_s, y_s), are known (Figure 1b):

$$v(x_k, y_k) = f(\boldsymbol{\theta}, x_k, y_k), \boldsymbol{\theta} = [x_s, y_s, \alpha_1, \alpha_2] \tag{1}$$

where $\alpha_1 = A\cos(\beta)$ and $\alpha_2 = A\sin(\beta)$ and function f is provided by the flow model, which computes the local flow velocity at the place of the sensor caused by the dipole source $\underline{\boldsymbol{\theta}}$. A potential flow generated by a dipole source is considered here, as assumed widely in the literature (Hassan 1993; Abdulsadda and Tan 2013). For the case in which the ALL sensors, the dipole source and the direction of the dipole vibration are all located in a same plane (x–y plane) parallel to the ALL body's cross-section, and in which the presence of body and sensors has negligible effect on the flow distribution (see more discussion in Abdulsadda and Tan 2013), the flow velocity at the sensor site (x_k, y_k) can be written as:

$$v(x_k, y_k) = \frac{a^3 v^d}{2{r_k}^5}((2(x_k - x_s)^2 - (y_k - y_s)^2)\cos\beta + 3(x_k - x_s)(y_k - y_s)\sin\beta) \tag{2}$$

where a is the dipole diameter and $v^d = A\sin(\omega t)$ represents the vibration of the dipole with maximum velocity of A and angular frequency ω. The value of ω is assumed to be known. Typically, each sensor can only measure the flow velocity component along a specific direction, which is assumed to be the case in this work. The signal amplitude for sensor k at frequency ω is extracted as the measurement M_k through, for example, fast Fourier transform, which can be written as:

$$M_k = f(\boldsymbol{\theta}, x_k, y_k) = \left| \frac{(2(x_k - x_s)^2 - (y_k - y_s)^2)\alpha_1 + 3(x_k - x_s)(y_k - y_s)\alpha_2}{2r_k^5/a^3} \right| \tag{3}$$

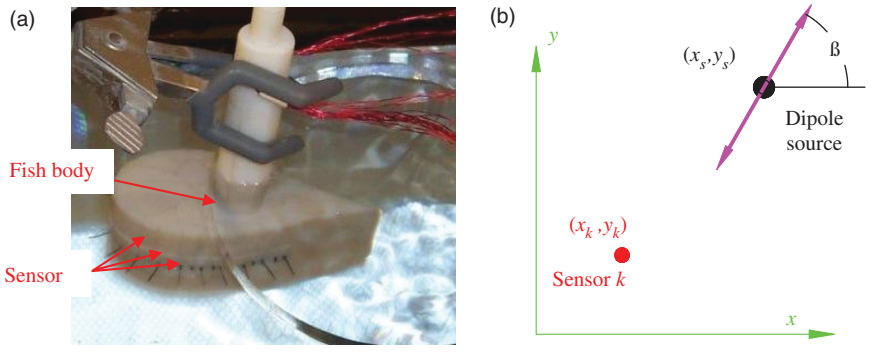

Figure 1. (a) A prototype of an artificial lateral line with sensors; (b) illustration of the dipole parameters.

where $\boldsymbol{\theta} = [x_s, y_s, \alpha_1, \alpha_2]$ characterizes the dipole source, including its location and vibration amplitude/orientation. In Equation (3), it is assumed that the sensors measure the x-component of the flow velocity. By exploitation of the proper rotation matrix, Equation (3) can be generalized to the case of an arbitrary sensing direction.

2.2. Dipole identification

Equation (3) demonstrates that the local flow speed can be determined if four parameters of the dipole are known. The ALL actually solves an inverse problem to identify the dipole, in which a dipole ($\boldsymbol{\theta}$) is sought such that the difference between the sensor measurements and the flow field generated by $\boldsymbol{\theta}$ is minimum. This means that the inverse problem can be converted as a minimization problem, as follows:

$$\begin{aligned} \text{Minimize} J(\boldsymbol{\theta}) &= \frac{\boldsymbol{M} - |\boldsymbol{f}(\boldsymbol{\theta}, \boldsymbol{x}, \boldsymbol{y})|}{\boldsymbol{M}} \\ \boldsymbol{M} &= [M_1, M_2, \ldots, M_{N_{\text{sensor}}}] \\ \boldsymbol{f}(\boldsymbol{\theta}, \boldsymbol{x}, \boldsymbol{y}) &= [f_1, f_2, f_3, \ldots, f_{N_{\text{sensor}}}], f_k = (\boldsymbol{\theta}, x_k, y_k) \end{aligned}$$

where M_k is the measured local flow velocity at the kth sensor (given) and $f_k(\boldsymbol{\theta}, x_k, y_k)$ is the theoretically computed flow velocity at the kth sensor using Equation (3). In the absence of uncertainties, the global minimum of the minimization problem is the actual dipole, at which the error function (J) is zero, *i.e.* ($\boldsymbol{\theta}^\star = \underline{\boldsymbol{\theta}}$) and $J(\boldsymbol{\theta}^\star) = 0$, unless $N_{\text{sensor}} < 4$. In the latter case, the number of equations is less than the number of unknown parameters; therefore, there could be an infinite number of $\boldsymbol{\theta}^\star$ which result in $J = 0$.

Owing to the presence of uncertainty in the sensor measurements and the inaccuracy of the flow model, in general, there is a difference between $\boldsymbol{\theta}^\star$ and $\underline{\boldsymbol{\theta}}$, called the identification error (e):

$$e = \left[\frac{\underline{x}_s - x_s^*}{1\text{cm}}, \frac{\underline{y}_s - y_s^*}{1\text{cm}}, \frac{\underline{\alpha}_{1s} - \alpha_{1s}^*}{1\text{cm/s}}, \frac{\underline{\alpha}_{2s} - \alpha_{2s}^*}{1\text{cm/s}} \right] \tag{4}$$

where the underlined quantities denote the parameters of the actual dipole. This equation defines the identification error as the Euclidean norm of $\boldsymbol{\theta}^\star - \underline{\boldsymbol{\theta}}$, which is made dimensionless to avoid dimension mismatch when calculating the norm. In general, $e \geq 0$ and, besides, $0 \leq J(\boldsymbol{\theta}^\star) \leq J(\underline{\boldsymbol{\theta}})$. This means that the actual location of the dipole is no longer the global minimum. For dipole identification, two sources of uncertainty can be identified: flow model uncertainty and sensor uncertainty. Most previous studies on dipole source localization/identification have not explicitly considered these factors or have accommodated only the sensor uncertainty (*e.g.* Abdulsadda and Tan 2011, 2013). In this study, the uncertainties introduced by both the flow model and the sensor measurement are incorporated into the ALL design systematically.

2.3. Simulation of uncertainties

Limited precision of the sensors introduces one type of uncertainty in the ALL system design. Since the measuring range of the sensor is fixed, the amount of uncertainty is assumed to be independent of the flow magnitude; therefore, it is simulated as an additive noise (Beyer and Meyer-Nieberg 2006):

$$M_k(\boldsymbol{\theta}) = |\underline{M}_k(\boldsymbol{\theta}) + \boldsymbol{\varepsilon}_{\text{sensor}} N(0,1)|, k = 1, 2, \ldots, N_{\text{sensor}} \tag{5}$$

where M_k is the indicated flow velocity by the kth sensor, while the true flow velocity is $\underline{M}_k$. The parameter $\boldsymbol{\varepsilon}_{\text{sensor}} \geq 0$ determines the noise strength of the sensor uncertainty. $N(0,1)$ is a random number sampled from the standard normal distribution.

Analytical methods typically depend on idealized assumptions or simplifications. Consequently, the actual velocity at a sensor location may be different from the one computed using a flow model. The difference between the actual and the predicted flow, often used in other engineering studies, as a fraction of the actual flow, is defined as follows:

$$\underline{M}_k(\underline{\boldsymbol{\theta}}) = |f_k(\underline{\boldsymbol{\theta}})| \times \exp(\boldsymbol{\varepsilon}_{\text{model}} N(0,1)), k = 1 \ldots, N_{\text{sensor}} \tag{6}$$

where $\underline{M}_k(\underline{\boldsymbol{\theta}})$ and $f_k(\underline{\boldsymbol{\theta}})$ are the actual flow velocity and the computed flow velocity according to the exploited flow model at the kth sensor, respectively. The parameter $\boldsymbol{\varepsilon}_{\text{model}} \geq 0$ determines the magnitude of the uncertainty in the flow model, as commonly used for simulation of a Gaussian noise (Hansen *et al.* 2009), which becomes equivalent to simple multiplicative noise for small values of $\varepsilon_{\text{model}}$.

Equations (5) and (6) enable simulation of the uncertainties in the identification process. Sensors measure the flow velocity of $\boldsymbol{M}$, which differs from the true value ($\underline{\boldsymbol{M}}$). On the other hand, an inaccurate flow model is utilized to interpret these inaccurate data. The identification error depends on many parameters, including the values of $\varepsilon_{\text{model}}$ and $\varepsilon_{\text{sensor}}$, N_{sensor}, and sensor locations and orientations.

To obtain a rough estimation of the values of $\varepsilon_{\text{sensor}}$ and $\varepsilon_{\text{model}}$, an underwater experiment and a computational fluid dynamic simulation were performed, from which values of $\varepsilon_{\text{sensor}} = 0.0015$ cm/s and $\varepsilon_{\text{model}} = 18\%$ were derived (Ahrari *et al.* 2015).

3. Design optimization

The ultimate goal of the ALL design optimization problem is to find the optimal shape and size of the body and the locations of sensors on its body such that a fitness measure ($g(\boldsymbol{X})$) of the design $\boldsymbol{X}$ is maximized.

3.1. Design parameters

The conformal mapping technique is used to describe a streamlined body (in this case, the cross-section profile of the cylindrical body) and the location of sensors on it. Consider the complex plane $\mathbb{C}$ and a point $\xi \in \mathbb{C}$. The following transformation maps ξ to z with respect to the transformation variable $\lambda \in \mathbb{R}$ (Panton 1984):

$$z = \xi + b^2/\xi, \xi = R\exp(i\beta) - \lambda, b = R - \lambda, \beta \in [-\pi, \pi) \tag{7}$$

Equation (7) defines a disk with radius R, offset along the real axis by $\lambda \in \mathbb{R}$. By choosing b, the disk can be mapped to a symmetrical, streamlined body. Therefore, R and λ specify the size and the shape of the body, and β_k denotes location of the kth sensor on the fish body. For $\lambda /R = 1$, the shape of the ALL is circular, while for $\lambda /R = 0$, the shape becomes a line. Other values between these two extremes result in a fish-like ALL.

Symmetry about the real axis is exploited to reduce the number of design variables, and thus the set of design variables, $\boldsymbol{X} = [X_1, X_2, \ldots, X_D]$, consists of:

- size variable: $X_{1\min} \leq X_1 = R \leq X_{1\max}$
- shape variable: $X_{2\min} \leq X_2 = \lambda/R \leq X_{2\max}$
- angular position of the first sensor on the fish body: $0 \leq X_3 = \beta_1 \leq \beta_{\max}$
- angular position of the kth sensor relative to the $(k-1)$th sensor: $0 \leq X_k = \beta_{k-2} - \beta_{k-1} \leq \beta_{\max}$, for $k = 4,5, \ldots, N_{\text{sensor}}/2$.

N_{sensor} specifies the total number of sensors in the ALL. Because of the symmetry about $y = 0$, only locations of the sensors on the top part of the body are independent parameters, and thus there are $2 + 0.5N_{\text{sensor}}$ design parameters, where N_{sensor} is an even number. For the rest of this study,

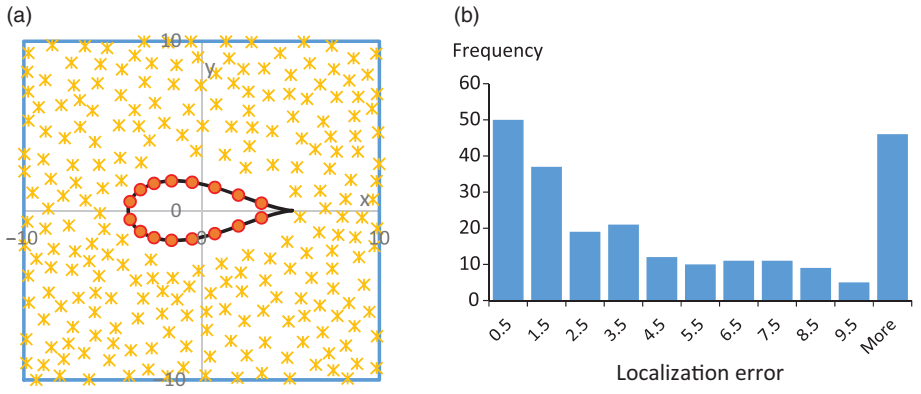

Figure 2. (a) Illustration of an artificial lateral line and a set of possible dipole locations; (b) an example histogram of the identification errors.

the following values for the range of design parameters are considered, unless mentioned otherwise: $X_{1\min} = 0.5\,\text{cm}$, $X_{1\max} = 4\,\text{cm}$, $X_{2\min} = 0$, $X_{2\max} = 1$ and $\beta_{\max} = 8\pi/N_{\text{sensor}}$.

3.2. Fitness function

The fitness function of each design needs to be computed to evaluate the 'goodness' of the design. The evaluation of the fitness function must take into account the fact that a dipole may lie anywhere in the predefined working area and may vibrate along any direction in the x–y plane. Since it is not feasible to consider all possible cases, the identification problem is solved for a finite number (N_{dipole}) of dipole locations. For the problem at hand, the bounds for dipole parameters ($\boldsymbol{U}_\theta$ and $\boldsymbol{D}_\theta$) are defined such that a dipole may lie anywhere outside the ALL, inside a square, and may vibrate in any directions, while the velocity of the dipole is larger than or equal to a minimum threshold, ($A \geq A_{\min}$). For the rest of this study, $A_{\min} = 3\,\text{cm/s}$, $\boldsymbol{U}_\theta = [10\ 10\ 10\ 10]$ and $\boldsymbol{D}_\theta = [-10, -10, -10, 0]$ are used (Figure 2a). Note that $[x, y, \alpha_1, \alpha_2]$ and $[x, y, -\alpha_1, -\alpha_2]$ are identical dipoles; therefore, the lower bound of α_2 was set to 0.

It is notable that the body of the ALL blocks wave propagation towards a sensor if some parts of it lie between the sensor and the dipole. Although these sensors may still provide some measurements, they are excluded from the identification process, as the simplistic potential flow model used here is not capable of capturing such complex flow phenomena.

For each chosen dipole setting, the inverse problem is solved and the identification error is computed (see an example in Figure 2). The distribution of all identification errors ($\boldsymbol{e} = [e_1, e_2, \ldots, e_{N\text{dipole}}]$) is then utilized to define the fitness function, $g(\boldsymbol{X})$. A simple and reasonable fitness function is then defined by averaging all identification errors together. However, the mean is not a robust statistic, since some outliers can significantly influence the calculated average (Figure 2b). Considering different sources of uncertainty, a robust performance measure based on the statistical distribution of e_i is strongly desired. The proposed fitness function follows this goal by giving higher weights (or credits) to more accurate identifications. The overall fitness is the mean of all the obtained credits:

$$g(\boldsymbol{X}) = \frac{1}{N_{\text{dipole}}} \sum_{i=1}^{N_{\text{dipole}}} \exp(-\zeta e_i^2) \tag{8}$$

In the above equation, parameter ζ determines how quickly the obtained credit reduces when the identification error increases. For fixed distribution of the identification errors, the calculated fitness increases if ζ is reduced. Selection of an appropriate value for this parameter is discussed later.

It is notable that because of sensor and flow model uncertainties, random selection of a finite number of dipoles and the random initial solution for the inverse problem, there is uncertainty in evaluation of the fitness, a matter which is common in robust optimization studies (Beyer and Sendhoff 2007; Kang, Lee, and Lee 2012). The fitness function $g(\boldsymbol{X})$ is a random function, which means that an independent evaluation of a design $\boldsymbol{X}$ leads to different values for $g(\boldsymbol{X})$, for which mean and standard deviation $(\bar{g}, s_g)$ can be computed. This uncertainty in fitness evaluation results in selection noise, in which a bad solution may be preferred over a better one. Selection noise can be reduced if the variance among the true fitness of designs is maximized or when the variance of the estimated fitness under independent evaluations is minimized. Accordingly, the selection reliability index (SRI) can be defined as follows (Ahrari *et al.* 2015):

$$\mathrm{SRI} = \frac{\mathrm{StDev}(\bar{\mathrm{g}})}{\mathrm{mean}(\mathrm{s}_g)} \tag{9}$$

A larger SRI usually refers to a smaller selection noise. A parameter study is performed in the next section to monitor the effect of different parameters on the SRI, which helps to select a reasonable parameter setting.

3.3. A bi-level optimization method

The fitness function formulated in the previous section is based on the values of the dipole identification errors. This means that for each design evaluation, the inverse problem, which is actually an optimization problem itself, must be solved many times. Consequently, the optimization process is bi-level, where the upper level optimizes all parameters of ALL ($\boldsymbol{X}$), while the lower level solves the inverse problem many times to obtain a robust estimate of the location and vibration angle of the dipole by minimizing $J(\boldsymbol{\theta})$, as follows:

$$\begin{aligned}
\text{Maximize } g(\boldsymbol{X}) &= \frac{1}{N_{\text{dipole}}} \sum_{i=1}^{N_{\text{dipole}}} \exp(-\zeta e_i^2) \\
\text{where } e_i &= \left[\frac{x_s - x_s^*}{1\text{cm}}, \frac{y_s - y_s^*}{1\text{cm}}, \frac{\alpha_{1s} - \alpha_{1s}^*}{1(\text{cm/s})}, \frac{\alpha_{2s} - \alpha_{2s}^*}{1(\text{cm/s})} \right]_i \\
\text{Subject to } \theta_i^* &= \text{argmin}\{J(\theta_i)\} \\
D_x \le X \le U_x, & \\
X_3 + X_4 + X_5 + \ldots + X_D \le \pi &
\end{aligned}$$

where $\boldsymbol{D_x}$ and $\boldsymbol{U_x}$ are the lower and upper bounds of the design parameters, respectively, and $g(\boldsymbol{X})$ is the fitness of the design $\boldsymbol{X}$, which is directly related to the identification accuracy. The linear constraint ensures that all the independent sensors are placed on the top of the ALL. The sensing direction of a sensor is assumed to be tangential to the body at the place of the sensor.

Bi-level optimization has been shown to be effective in many practical and even multi-objective optimization problems (Deb and Sinha 2009; Linnala *et al.* 2012), although it has been criticized for being complex and hard even when the problems in both levels are linear (Colson, Marcotte, and Savard 2007). The situation is more challenging for the problem at hand owing to the presence of nonlinearities at both levels and the presence of uncertainties, which can be somewhat mediated by proper choice of the inverse solver.

3.3.1. Inverse solver (lower level)

The challenge of high computation of bi-level optimization can be moderated by selecting a fast optimization method for the lower level, especially for the problem at hand, where the inverse solver

should be run several hundred times per design evaluation in the upper level. In this study, the Newton–Raphson (N-R) method is selected for the lower level. This method was demonstrated to be a reliable tool for dipole source localization (Abdulsadda and Tan 2013); however, some changes are required since there are terms in $J(\boldsymbol{\theta})$ involving absolute values, which means that the gradient of $J(\boldsymbol{\theta})$ is not defined at certain points. The N-R-based method employed in this study starts the search from a semi-random initial solution ($\boldsymbol{\theta}_{\text{ini}}$):

$$\boldsymbol{\theta}_{\text{ini}} = \underline{\boldsymbol{\theta}} + \alpha_\theta(\boldsymbol{U}_\theta - \boldsymbol{D}_\theta) \otimes \boldsymbol{r} \tag{10}$$

where $\boldsymbol{r}$ is vector of four uniformly distributed random numbers in $[-0.5, 0.5]$, $\boldsymbol{U}_\theta$ and $\boldsymbol{D}_\theta$ are the upper and lower bounds for the dipole parameters, respectively, α_θ specifies the relative size of the region around the true dipole parameters, and the notation $\otimes$ refers to element-wise multiplication. For this study, $\alpha_\theta = 0.5$ is used.

A line search is performed along the best direction: $\mathbf{d}_{\text{best}} = -\mathbf{H}^{-1}(\text{J}) \times \nabla\text{J}$, where $\mathbf{H}$ and ∇ denote the Hessian matrix and the gradient vector, respectively, using the golden section search, with an initial step size of Δ. $J(\boldsymbol{\theta}_{\text{ini}})$, $J(\boldsymbol{\theta}_{\text{ini}} + \Delta \times \boldsymbol{d}_{\text{best}})$ and $J(\boldsymbol{\theta}_{\text{ini}} - \Delta \times \boldsymbol{d}_{\text{best}})$ are computed. If the last term is the smallest, moving along $\boldsymbol{d}_{\text{best}}$ increases $J(\boldsymbol{\theta})$; therefore, $\boldsymbol{d}_{\text{best}}$ is inverted. This may happen because of multi-modality or the absence of derivatives at some points. The line search terminates after a maximum of N_{J} evaluations of $J(\boldsymbol{\theta})$, or when the step size is too small (smaller than 10^{-4} used in this study) to make considerable changes in $J(\boldsymbol{\theta})$. The parameter $\boldsymbol{d}_{\text{best}}$ is then updated. This process continues until the predefined number of evaluations of $J(\boldsymbol{\theta})$ for a single run of the inverse solver (*maxJeval*) is consumed. The inverse solver is also terminated if the difference between the initial and final solutions in a line search loop is smaller than 10^{-4}; therefore, the actual number of evaluations of $J(\boldsymbol{\theta})$ (*usedJeval*) can be smaller than *MaxJeval*.

Based on the preliminary results, computation of $\boldsymbol{d}_{\text{best}}$ appeared to be about five times costlier than evaluation of $J(\boldsymbol{\theta})$. Therefore, the value of *usedJeval* is increased by five whenever $\boldsymbol{d}_{\text{best}}$ is updated. *MaxJeval* and N_{J} are chosen to be large enough to allow the algorithm to converge, but not too large to result in unnecessary increases in computational cost. A parameter study is performed in Section 3.4 to decide on the values of these parameters.

It is noted that N-R is a local search method. Furthermore, there are some points where the function $J(\boldsymbol{\theta})$ is not analytical. This means that there is no guarantee that the inverse solver can find the global optimum ($\boldsymbol{\theta}^\star$), especially in the presence of noise. One alternative, which is adopted in this article, is to solve the inverse problem N_{inverse} times with different initial solutions ($\boldsymbol{\theta}_{\text{ini}}$) for a given set of measurements M, which leads to N_{inverse} estimated values for the dipole source. Among them, the one with the minimum J is selected as the localized dipole. The effect of N_{inverse} is investigated in Section 3.4.

3.3.2. Upper-level optimization method

Since the landscape of the $g(\boldsymbol{X})$ is unknown and derivatives of $g(\boldsymbol{X})$ are not explicitly available, a metaheuristic that can handle multimodality, correlation and especially noise in the fitness function is preferred. A variant of the covariance matrix adaptation evolution strategy (CMA-ES) (Hansen and Ostermeier 2001; Hansen 2009) is employed to perform optimization at the upper level, considering its promising results in the BBOB2009 optimization workshop on noisy test problems (Auger *et al.* 2010). CMA-ES belongs to the category of evolution strategies that adapt the full covariance matrix, which makes it an efficient method for handling correlation among design variables. The only problem-dependent control parameter of CMA-ES is the population size. A dynamic update of population size is preferred in this study, which will be discussed in Section 3.4.

3.4. Parameter study

To use the proposed bi-level algorithm, one should decide on the values of ζ in the fitness function, the evaluation budget for one run of the inverse solver (*MaxJeval*), the maximum number of calls

of $J(\boldsymbol{\theta})$ in the line search in the inverse solver (N_J), the number of dipoles over which $g(\boldsymbol{X})$ is evaluated (N_dipole), and the number of times the inverse problem is solved for a given dipole and a set of sensor measurements with different initial solutions (N_inverse). The goal is to find the set of these parameters such that the identification accuracy and SRI are maximized, while the computation cost is minimized. For this purpose, 100 random designs ($\boldsymbol{X}_1, \boldsymbol{X}_2, \ldots, \boldsymbol{X}_{100}$) are generated. Since there are many parameters, a few are studied at a time, while the rest are set to some default values unless mentioned otherwise. The default values, obtained using a preliminary parameter study, are as follows: $N_\mathrm{dipole} = 1024$, $N_\mathrm{inverse} = 1$, $N_\mathrm{inverse} = 1$ and $\zeta = 1$.

To demonstrate the flexibility and robustness of the proposed optimization method, and to analyse the effect of the extent of uncertainty on the optimized design, three distinct cases are considered for the rest of this study:

- Case I: Ideal case with $\varepsilon_\mathrm{model} = \varepsilon_\mathrm{sensor} = 0$,
- Case II: Low uncertainty with $\varepsilon_\mathrm{model} = 0.01$ and $\varepsilon_\mathrm{sensor} = 0.0015$ cm/s
- Case III: High uncertainty with $\varepsilon_\mathrm{model} = 0.20$ and $\varepsilon_\mathrm{sensor} = 0.0015$ cm/s.

Parameter study and optimization results are investigated for these three cases. Increasing N_inverse predictably increases the identification accuracy, as demonstrated in Ahrari *et al.* (2015); however, the computational time grows proportionally. One interesting finding in Ahrari *et al.* (2015) was that the effect of increasing N_inverse is similar for all designs. This means that if $g(\boldsymbol{X}_1) > g(\boldsymbol{X}_2)$ for $N_\mathrm{inverse} = 1$, the probability that $g(\boldsymbol{X}_1) < g(\boldsymbol{X}_2)$ for other values of N_inverse is small, *i.e.* the rank of solutions does not change if N_inverse is changed. Since selection in CMA-ES is performed according to the rank of solutions, the optimization can be performed with $N_\mathrm{inverse} = 1$ to minimize the computational cost. The obtained optimum design is then used with $N_\mathrm{inverse} > 1$ in practice to increase the identification accuracy.

3.4.1. Effect of maxJeval and N_J

Parameters *maxJeval* and N_J control the inverse solver by limiting the overall computation budget and computation budget per line search step, respectively. Improper selection of these parameters may lead to premature interruption of the inverse solver or excessive but unnecessary computation. To investigate the effect of *maxJeval* and N_J on the identification accuracy, the randomly generated designs are evaluated using different values for these parameters. Figure 3 illustrates the mean fitness of 100 random designs for Cases I, II and III. Note that the actual computation (*usedJeval*) can be smaller than *maxJeval*, because the inverse solver employs some statistical criteria to abort whenever it is predicted that further search cannot result in significant change in the solution.

It can be observed that:

- The average fitness increases when *maxJeval* is increased. This effect is spectacular in Case I, significant in Case II, but insignificant in Case III.
- For Cases I and II, increasing N_J up to a certain point (about $N_J = 15$) improves the fitness of the designs. After that, it has no significant effect.
- A huge decline in the average fitness of the design is observed when the amount of uncertainty increases. For instance, the average fitness is much higher in Case II (low uncertainty) than in Case III (high uncertainty).
- The growth of *usedJeval* with *maxJeval* is slower than linear. Since computation time is proportional to *usedJeval*, the trade-off between *maxJeval* and identification accuracy suggests not sacrificing the fitness for a smaller *maxJeval*.

Based on the results from this section, values of *maxJeval* $= 1600$ and $N_J = 30$ are set for the rest of this study.

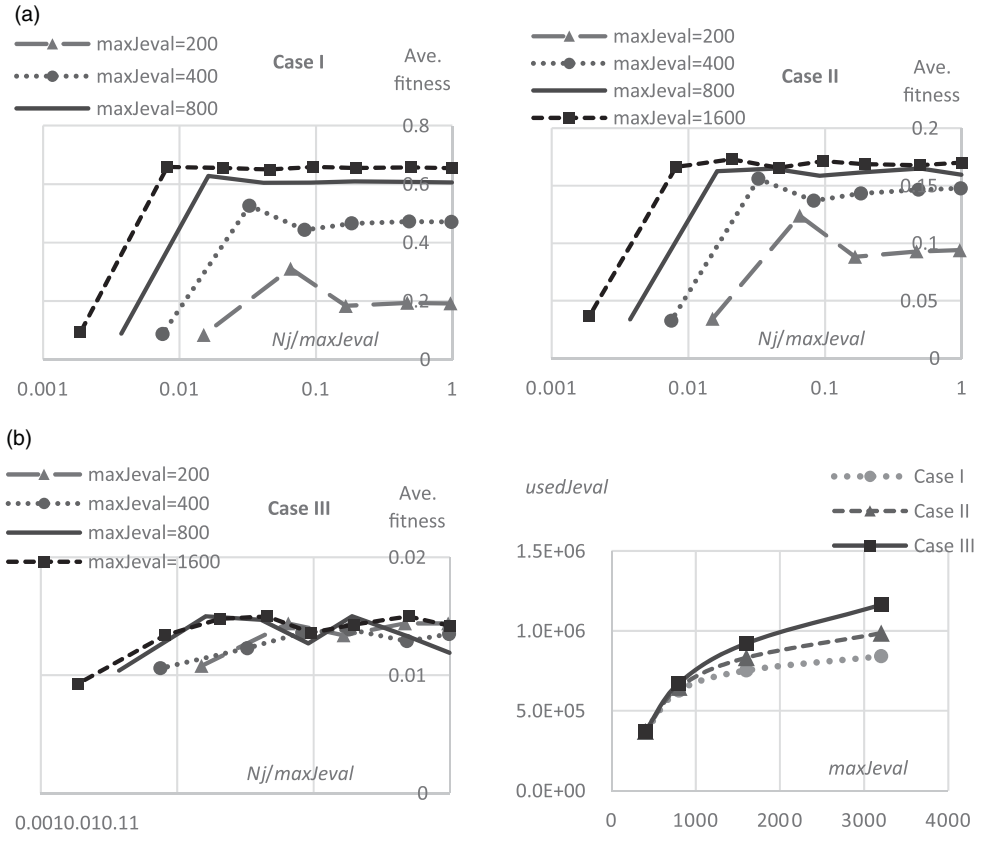

Figure 3. Average fitness of 100 random designs for different values of *maxJeval* and N_J in (a) Case I, (b) Case II, and (c) Case III; (d) average *usedJeval* for different values of *maxJeval* for different cases with $N_{\text{dipole}} = 1024$.

3.4.2. Effects of population size, N_{dipole} and ζ

In this study, problem-specific population sizing for CMA-ES is adopted, in which the population size is reduced dynamically while N_{dipole} is increased with the iteration counter. The justification is that in early iterations, a large population size allows an enhancement in exploration of the algorithm; however, a small value for N_{dipole} keeps the computational time in a reasonable range. While this strategy is useful for the initial stage of the algorithm, owing to the presence of high uncertainty in $g(\boldsymbol{X})$, the progress rate of the search algorithm near the optimal solution becomes zero before the population converges to the exact location of the optimum (Beyer and Meyer-Nieberg 2006). To address this problem, N_{dipole} is dynamically increased to reduce the standard deviation of $g(\boldsymbol{X})$. At the same time, the population size is reduced. The evaluation budget of the whole optimization process is specified in terms of the number of times the inverse problem is solved (*MaxInvSolve*). When one-third of the evaluation budget is consumed, the population size is halved, while N_{dipole} is doubled. This is performed again when two-thirds of the evaluation budget is consumed. Based on a preliminary parameter study, the initial population size and *MaxInvSolve* are set to 180 and 2×10^6, respectively.

Parameter ζ also affects the selection noise; too small or too a large value may reduce the variation of fitness among different solutions; however, practical requirements, *e.g.* the demanded identification accuracy, should also be considered while setting this parameter. When the uncertainty is high, the expectation of the identification accuracy should be less; however, to compare the effect of uncertainties on the fitness of the optimized design in different cases, a fixed value of $\zeta = 0.1$ is used for the rest of this study.

4. Numerical results

4.1. Case studies

Three simulation studies are performed to analyse the effectiveness of the proposed optimization tool in these specific cases, where the final solution is checked with engineering intuition. For this purpose, the optimization algorithm is run for Cases I, II and III, while the dipoles are relocated so that they lie only on the left (mode a), right (mode b) or top and bottom (mode c) of the ALL. For these trials, $N_{\text{sensor}} = 12$ is used. Figure 4 illustrates the arithmetic mean of the final designs in 10 independent runs for each case.

- For Cases IIa and IIIa, most sensors have moved to the right side of the fish body to maximize the average number of sensors that can receive a signal from the dipoles. In contrast, for Cases IIb and IIIb, most sensors have moved to the left side for the same reason.
- The final solutions for Cases IIc and IIIc are totally different. The sensors are quite uniformly distributed on the ALL and, besides, the ALL is highly stretched, probably to maximize the spread of sensors so that most of them can still receive a signal from the dipoles on the same side.
- The optimized design of Case I has a comparatively small size and does not show any significant variation with respect to the locations of the dipoles. This could be due to the fact that since there are four unknown parameters in the inverse problem, only measurements from four sensors are required to solve the inverse problem. If the measurements are completely accurate, neither extra sensor measurements nor diversity in the location of the sensors would provide more information on parameters of the dipole. One justification for the small size of the ALL may be maximization of the number of sensors that can receive a signal, so that for all dipoles at least four sensors can provide a signal.

These results demonstrate that in all cases, there is good agreement between the final designs found by the optimization method and the one predicted by engineering intuition. The optimal designs strongly depend on the locations of the dipoles. More importantly, the optimization method can reliably find the optimal design parameters with respect to the defined objective function for each case, although it becomes harder when uncertainty, and thus the selection noise, is exacerbated.

4.2. Generative bi-objective optimization

In this section, it is assumed that dipoles may lie anywhere in the 20 × 20 cm tank, the ultimate case within the scope of this study. Furthermore, two constraints are imposed by practical requirements. First, the lower limit of $X_2 = \lambda/R$ is increased to 0.1 to prevent very flat designs that are not practical.

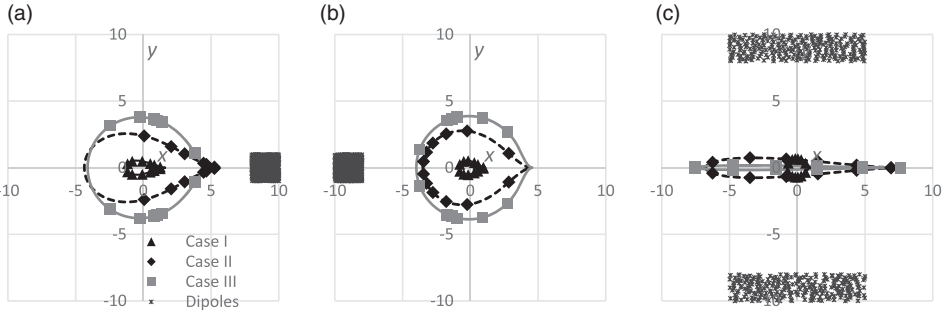

Figure 4. Mean of the final designs from 10 independent runs for Cases I, II and III, when dipoles are (a) on the right, (b) on the left, and (c) on the top and bottom of the artificial lateral line. The units of both the horizontal and vertical axes are centimetres.

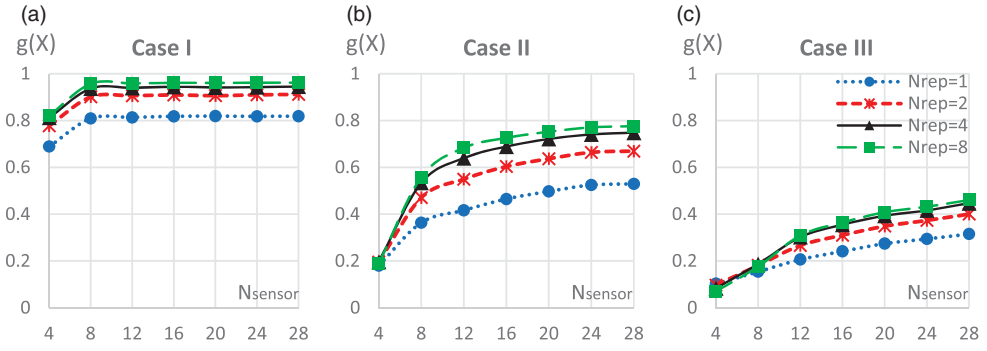

Figure 5. Trade-off between fitness and N_{sensor}: (a) Case I, (b) Case II, and (c) Case III.

Secondly, in contrast to the setting so far which excludes the dipoles that lie inside or very close to the fish body, zero credit is given for such dipoles. This implicitly penalizes a larger ALL, since it receives more zero credits, thereby reducing the overall fitness. This counteracts the undesirable advantage of larger ALLs, which occupy a larger fraction of the search space and leave a small region for dipoles to lie in. Predictably, increasing N_{sensor} can increase the fitness of the final design, since it provides more data on the dipole; however, fabrication cost and integration complexity increase with the number of sensors. The trade-off between N_{sensor} and $g(\boldsymbol{X})$ can be analysed by performing a bi-objective optimization in which the second objective is minimization of N_{sensor}. Practically, a limited option for the number of sensors is worth considering, *e.g.* $N_{\text{sensor}} \leq 30$ and N_{sensor} is an even number. This provides motivation for running the single-objective optimization problem with different values of N_{sensor} instead of running a bi-objective optimization.

Each optimization problem is solved 10 times independently and the final solutions from the optimization runs are re-evaluated again with $N_{\text{dipole}} \approx 10{,}000$ for different values of N_{inverse}. Figure 5 plots the obtained trade-off front for each case and some selected values of N_{sensor}. Figure 6 depicts the shape and size of five designs representing the distribution of the 10 final solutions. The parameters of these designs are the pth percentile of the corresponding parameters in the final solutions. For example, the parameters of the 50% percentile design are the median of the corresponding parameters in the final solutions. This may show whether the algorithm has converged to similar solutions. Based on the obtained results, the following conclusions can be drawn:

- Figure 5 demonstrates that increasing N_{sensor} always improves the fitness, except for Case I after $N_{\text{sensor}} = 8$, and thus a knee in the Pareto front is observed. This knee emerges at $N_{\text{sensor}} = 12$ for Case II. For Case III, in contrast, no knee can be detected and the slope of the curve remains quite high everywhere. This implies that when the amount of uncertainty increases, the contribution of extra sensors becomes more significant.
- In Case I when $N_{\text{sensor}} \geq 8$ (Figure 5), the fitness of the optimized design is close to 1 when N_{sensor} is great. This means that the identification error for any arbitrary dipole is almost zero. Note that zero credit is assigned if a dipole is located inside or very close to the fish body; therefore, it is impossible to reach a fitness of one.
- Increasing N_{sensor} (Figure 5) has a significant positive effect on the identification accuracy. In practice, the inverse solver should be run multiple (*e.g.* more than four) times to maximize identification accuracy. This effect can be observed for all the cases.
- The similarity of the shape and size of the final designs for a fixed N_{sensor} in independent runs (Figure 6) confirms the reliability of the optimization results. Case II with $N_{\text{sensor}} = 16$ is an exception, in which a few runs have converged to a circular ALL. It seems that for this case there are two (near-)global minima with almost identical fitness.

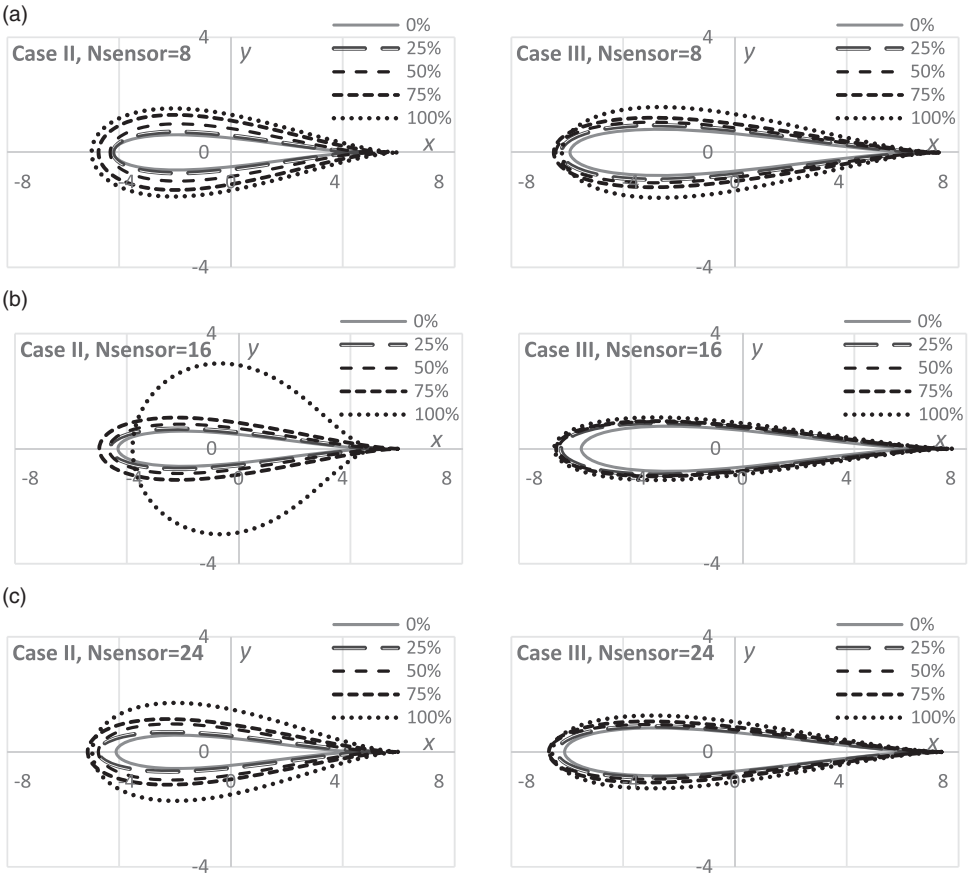

Figure 6. Representation of final solutions for Cases II and III: (a) $N_{sensor} = 8$, (b) $N_{sensor} = 16$, and (c) $N_{sensor} = 24$. Parameters of each illustrated solution are the pth percentile of the corresponding parameters of the final solutions from 10 independent runs.

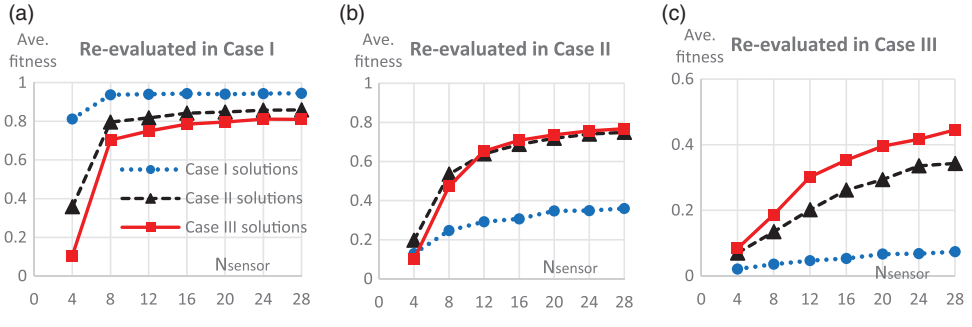

Figure 7. Average fitness of the optimized designs in different cases re-evaluated ($N_{inverse} = 4$) for (a) Case I, (b) Case II, and (c) Case III.

4.3. Importance of the uncertainty amount

Optimized designs from each case are re-evaluated in other cases to investigate fitness degradation caused by ignoring the effect of the amount of uncertainty in the optimization process. Figure 7 illustrates the average fitness of the optimized designs from different cases, re-evaluated for conditions of all cases.

According to Figure 7, the optimized solution of each case is the optimal one for that case only. For example, if the conditions of Case III are applied in practice, solutions from Case III are the best choice, solutions from Case II have lower fitness and solutions from Case I are far behind the other two cases. Similar conclusions can be drawn for other situations, with a small exception: if the condition of Case II is applied in practice, solutions from Cases II and III are almost equally fitted if $N_{\text{sensor}} \geq 12$, although their design parameters differ significantly.

4.4. Simultaneous bi-objective optimization

Solving the optimization problem for each value of N_{sesnor} has a flip side. The knowledge obtained through previous runs is overlooked since each run is independent from the others. Alternatively, one may attempt to find multiple and differently sized designs by optimizing both objectives simultaneously. In this study, one of the most successful multi-objective optimization methods, the non-dominated sorting genetic algorithm (NSGA-II) (Deb *et al.* 2002), is employed for this purpose. The maximum and minimum number of sensors is set to 8 and 32, respectively. To determine the number and location of sensors present in the design, the range of variables pertaining to sensor locations is extended to include negative values, for example $-A < X_4 < A$, so that the absence of a sensor can be determined from the negative value of X_4.

For this case, a more accurate evaluation of a design is required since, unlike the CMA-ES procedure, NSGA-II is an elitist method, and the error in the fitness evaluation of a design may remain until the end of the optimization process; therefore, N_{dipole} is set to 1024. The population size and *MaxInvSolve* for NSGA-II are set to 180 and 10^7, respectively. Although the evaluation budget is five times that of CMA-ES with a fixed value of N_{sensor}, the overall computation is less since one run of NSGA-II replaces several independent runs of CMA-ES with different values of N_{sensor}. The continuous variant is employed with recommended parameter setting ($\eta_c = \eta_m = 5, Pc = 0.9, P_m = 1/N$).

The final solutions from NSGA-II are re-evaluated and the trade-off fronts obtained using CMA-ES and NSGA-II methods are illustrated in Figure 8 for $N_{\text{inverse}} = 2$. The figure reveals that the trade-off front from NSGA-II is identical to that of CMA-ES. This indicates that the trade-off front obtained may be the true optimal one and there is no need for one-by-one computation of each trade-off solution; instead, the use of a bi-objective NSGA-II is able to find multiple trade-off solutions in a single simulation. Average values of the size variable ($X_1 = R$) and shape variable ($X_2 = \lambda/R$) in the final solutions of both methods are illustrated in Figure 9, which demonstrates that:

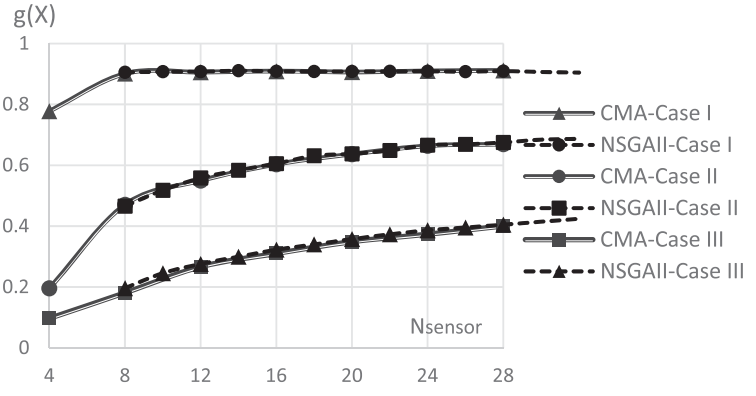

Figure 8. Trade-off fronts obtained from the non-dominated sorting genetic algorithm (NSGA-II) and covariance matrix adaptation evolution strategy (CMA-ES) for different cases.

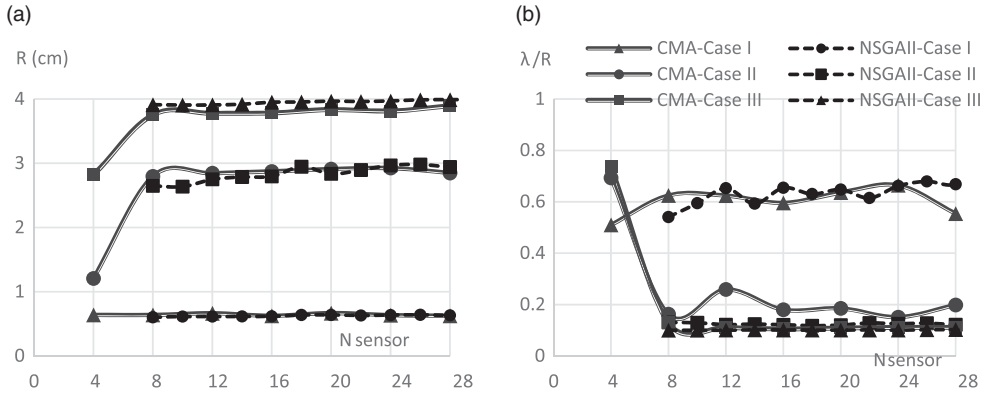

Figure 9. Final solutions using the covariance matrix adaptation evolution strategy (CMA-ES) and non-dominated sorting genetic algorithm (NSGA-II) for different cases: values of (a) size and (b) shape parameters.

- The optimal shape changes from circular with small R to flat with large R as the amount of uncertainty increases.
- For Case III, the shape variable ($X_2 = \lambda/R$) has reached the lower limit while R has reached its upper limit.
- For a fixed number of sensors and uncertainty amount, the final solutions of the NSGA-II and CMA-ES are similar.

It can be concluded that when the number of sensors (N_{sensor}) is flexible, NSGA-II is a more reasonable tool for finding a trade-off between the objectives for a fairly large range of N_{sensor}. A bi-criterion decision-making method can now be employed to choose a single preferred solution from the trade-off set. None of the three cases exhibits any knee-like region, indicating that there is no obvious choice for a particular solution in the ALL system design problem. A reference-point based approach (Wierzbicki 1980) or other multiple-criteria decision making-based methods (Miettinen 1999) would have to be used for choosing a single preferred solution.

5. Conclusions

The optimal design of an ALL system is a challenging task and it demands specialized algorithms to handle different sources of uncertainty. In this research, two different sources of uncertainty have been considered in solving the inverse problem of localizing a dipole source based on flow measurements at multiple sensor sites. A robust parametric fitness function has been proposed so that the uncertainty in fitness evaluation is minimized. Thereafter, a bi-level optimization method has been proposed and employed to optimize parameters of the ALL, including shape, size of the lateral line and placement of the sensors over the body. Several numerical studies have been performed to investigate the effect of the parameters of the algorithm. The recommended parameter settings are then derived from the results of these studies.

To show the flexibility of the method and effect of uncertainty on the optimized design, three cases with different magnitudes of uncertainty have been considered. The developed optimization method has been first validated by a sensitivity analysis in which dipoles are placed at particular regions of the search space, so that an intuitive prediction of placement of sensors can be obtained. The lateral line has subsequently been optimized for different numbers of sensors to monitor the trade-off between the number of sensors and the accuracy of identification. A comparison among the results of different cases demonstrated that the amount of uncertainty not only significantly influences identification accuracy but also varies the optimal ALL system. Increasing the number of sensors monotonically

and predictably boosts the identification accuracy; however, the gain after a certain point, called the knee, becomes insignificant. The recommended value of the number of sensors, based on the trade-off between the fitness and the number of sensors, increases as the amount of uncertainty increases, and for the case with the largest amount of uncertainty, no knee-like point could be observed for the tested range of number of sensors.

The dependency of the optimized design on the number of sensors and the amount of uncertainty highlights the importance of considering these factors in the design process, which, in most cases, can hardly be rendered by engineering intuition. It was also observed that the final solutions from each case can be the optimal ones only for that case, and significant fitness degradation is observed if these solutions are used in other conditions. Future research in the domain of this study includes extension of the proposed optimization method to the case in which the ALL system could localize a dipole in three-dimensional space, or when the dipole is moving, instead of vibrating. The authors also plan to prototype the obtained optimal design and conduct experiments to validate the numerical results. It is worth noting that the proposed methodology can also be utilized in other problems requiring optimal sensor placement, such as in structural health monitoring.

Acknowledgements

Computational work in support of this research was performed at Michigan State University's High Performance Computing (HPCC) Facility. Any opinions, findings and conclusions or recommendations expressed in this material are those of the authors and do not necessarily reflect the views of the National Science Foundation or the Office of Naval Research.

Disclosure statement

No potential conflict of interest was reported by the authors.

Funding

This material is based in part upon work supported by the National Science Foundation [Cooperative Agreement no. DBI-0939454] and by the Office of Naval Research [N000141210149, N000141512246].

References

Abdulsadda, A. T., and X. Tan. 2011. "Underwater Source Localization Using an IPMC-Based Artificial Lateral Line." Proc. of 2011 IEEE International Conference on Robotics and Automation. Shanghai, China. 2719–2724.

Abdulsadda, A. T., and X. Tan. 2012. "An Artificial Lateral Line System Using IPMC Sensor Arrays." *International Journal of Smart and Nano Materials* 3 (3): 226–242.

Abdulsadda, A. T., and X. Tan. 2013. "Nonlinear Estimation-Based Dipole Source Localization for Artificial Lateral Line Systems." *Bioinspiration & Biomimetics* 8 (2): 026005-1–15.

Ahrari, A., H. Lei, M. A. Sharif, K. Deb, and X. Tan. 2015. "Design Optimization of Artificial Lateral Line System Under Uncertain Conditions." Proc. of IEEE congress on Evolutionary Computation (CEC 2015). Sendai, Japan, (to appear): IEEE.

Auger, A., S. Finck, N. Hansen, and R. Ros. 2010. BBOB 2009: Comparison Tables of all Algorithms on all Noisy Functions. Technical Report, RT-0384, INRIA.

Beyer, H. G., and Meyer-Nieberg, S. 2006. "Self-Adaptation of Evolution Strategies Under Noisy Fitness Evaluations." *Genetic Programming and Evolvable Machines* 7 (4): 295–328.

Beyer, H. G., and B. Sendhoff. 2007. "Robust Optimization—A Comprehensive Survey." *Computer Methods in Applied Mechanics and Engineering* 196 (33): 3190–3218.

Bleckmann, H. 1994. *Reception of Hydrodynamic Stimuli in Aquatic and Semiaquatic Animals*. Stuttgart: Gustav Fischer Verlag.

Bleckmann, H. 2008. "Peripheral and Central Processing of Lateral Line Information." *Journal of Comparative Physiology A* 194 (2): 145–158.

Bleckmann, H., A. Przybilla, A. Klein, A. Schmitz, S. Kunze, and C. Brücker. 2012. "Station Holding of Trout: Behavior, Physiology and Hydrodynamics." In *Nature-Inspired Fluid Mechanics*, edited by C. Tropea and H. Bleckmann, 161–177. Berlin: Springer.

Chambers, L. D., O. Akanyeti, R. Venturelli, J. Ježov, J. Brown, and M. Kruusmaa, et al. 2014. "A Fish Perspective: Detecting Flow Features While Moving Using an Artificial Lateral Line in Steady and Unsteady Flow." *Journal of the Royal Society Interface* 11 (99): 20140467-1–13.

Colson, B., P. Marcotte, and G. Savard. 2007. "An Overview of Bilevel Optimization." *Annals of Operations Research* 153 (1): 235–256.

Coombs, S., and R. A. Conley. 1997a. "Dipole Source Localization by Mottled Sculpin. I. Approach Strategies." *Journal of Comparative Physiology A* 180 (4): 387–399.

Coombs, S., and R. A. Conley. 1997b. "Dipole Source Localization by Mottled Sculpin. II. The Role of Lateral Line Excitation Patterns." *Journal of Comparative Physiology A* 180 (4): 401–415.

Dagamseh, A. M. K., T. S. J. Lammerink, M. L. Kolster, C. M. Bruinink, R. J. Wiegerink, and G. J. M. Krijnen. 2010. "Dipole-Source Localization Using Biomimetic Flow-Sensor Arrays Positioned as Lateral-Line System." *Sensors and Actuators A* 162 (2): 355–360.

Deb, K., A. Pratap, S. Agarwal, and T. Meyarivan. 2002. "A Fast and Elitist Multiobjective Genetic Algorithm: NSGA-II." *IEEE Transactions on Evolutionary Computation* 6 (2): 182–197.

Deb, K., and A. Sinha. 2009. "Solving Bilevel Multi-objective Optimization Problems Using Evolutionary Algorithms." In *Evolutionary Multi-Criterion Optimization*, 110–124. Berlin: Springer.

DeVries, L., F. Lagor, H. Lei, X. Tan, and D. Paley. 2015. "Distributed Flow Estimation and Closed-Loop Control of an Underwater Vehicle with a Multi-modal Artificial Lateral Line." *Bioinspiration & Biomimetics* 10 (2): 025002-1–16.

DeVries, L., and D. A. Paley. 2013. "Observability-Based Optimization for Flow Sensing and Control of an Underwater Vehicle in a Uniform Flowfield." Proc. of American Control Conf. Washington, DC. 1386–1391.

Engelmann, J., W. Hanke, J. Mogdans, and H. Bleckmann. 2000. "Hydrodynamic Stimuli and the Fish Lateral Line." *Nature* 408 (6808): 51–52.

Fernandez, V. I., A. Maertens, F. M. Yaul, J. Dahl, J. H. Lang, and M. S. Triantafyllou. 2011. "Lateral-Line Inspired Sensor Arrays for Navigation and Object Identification." *Marine Technology Society Journal* 45 (4): 130–146.

Hansen, N. 2009. "Benchmarking a Bi-population CMA-ES on the BBOB-2009 Noisy Testbed." Proc. of the 11th Annual Conference Companion on Genetic and Evolutionary Computation Conference: Late Breaking Articles. Montreal, Canada, ACM. 2397–2402.

Hansen, N., S. Finck, R. Ros, and A. Auger. 2009. "Real-Parameter Black-Box Optimization Benchmarking 2009: Noisy Functions Definitions." RR-6869, inria-00369466.

Hansen, N., and A. Ostermeier. 2001. "Completely Derandomized Self-Adaptation in Evolution Strategies." *Evolutionary Computation* 9 (2): 159–195.

Hassan, E. S. 1993. "Mathematical Description of the Stimuli to the Lateral Line System of Fish Derived from a Three-Dimensional Flow Field Analysis." *Biological Cybernetics* 66 (5): 443–452.

Kang, J. S., T. Y. Lee, and D. Y. Lee. 2012. "Robust Optimization for Engineering Design. Engineering Optimization." *Engineering Optimization* 44 (2): 175–194.

Linnala, M., E. Madetoja, H. Ruotsalainen, and J. Hämäläinen. 2012. "Bi-level Optimization for a Dynamic Multiobjective Problem." *Engineering Optimization* 44 (2): 195–207.

Miettinen, K. 1999. *Nonlinear Multiobjective Optimization*. Boston, MA: Kluwer.

Panton, R. L. 1984. *Incompressible Flow*. Hoboken, NJ: John Wiley and Sons.

Pitcher, T. J., B. L. Partridge, and C. S. Wardle. 1976. "A Blind Fish Can School." *Science* 194: 963–965.

Ren, Z., and K. Mohseni. 2012. "A Model of the Lateral Line of Fish for Vortex Sensing." *Bioinspiration & Biomimetics* 7 (3): 036016-1–14.

Venturelli, R., O. Akanyeti, F. Visentin, J. Ježov, L. D. Chambers, and G. Toming, et al. 2012. "Hydrodynamic Pressure Sensing with an Artificial Lateral Line in Steady and Unsteady Flows." *Bioinspiration & Biomimetics* 7 (3): 036004-1–12.

Von Campenhausen, C., I. Riess, and R. Weissert. 1981. "Detection of Stationary Objects by the Blind Cave Fish Anoptichthys Jordani (Characidae)." *Journal of Comparative Physiology* 143 (3): 369–374.

Wierzbicki, A. P. 1980. "The use of Reference Objectives in Multiobjective Optimization." In *Multiple Criteria Decision Making Theory and Application*, 468–486. Berlin: Springer.

Yang, Y., N. Nguyen, N. Chen, M. Lockwood, C. Tucker, H. Hu, H. Bleckmann, C. Liu, and D. L. Jones. 2010. "Artificial Lateral Line with Biomimetic Neuromasts to Emulate Fish Sensing." *Bioinspiration & Biomimetics* 5 (1): 016001-1–9.